Homogeneous and heterogeneous nucleation of skyrmions in thin layers of cubic helimagnets

A. O. Leonov[1,2,3,*] and K. Inoue[1,2]

[1]*Chirality Research Center, Hiroshima University, Higashi-Hiroshima, Hiroshima 739-8526, Japan*

[2]*Department of Chemistry, Faculty of Science, Hiroshima University Kagamiyama, Higashi Hiroshima, Hiroshima 739-8526, Japan*

[3]*IFW Dresden, Postfach 270016, D-01171 Dresden, Germany*

(Received 19 March 2018; revised manuscript received 21 May 2018; published 6 August 2018)

Formation of isolated chiral skyrmions by homogeneous and heterogeneous nucleation has been studied in thin layers of cubic helimagnets via elongation of torons and chiral bobbers, respectively. Both torons and bobbers are localized in three dimensions, contain singularities, and, according to the theoretical analysis within the standard phenomenological models, can exist as metastable states in saturated and modulated phases of noncentrosymmetric ferromagnets. Their elongation into the defect-free skyrmion filament is facilitated by small anisotropic contributions making skyrmion cores negative with respect to the surrounding parental state. We show that isolated magnetic torons pose the same problem of compatibility with a surrounding phase as the torons in confinement-frustrated chiral nematics [I. I. Smalyukh *et al.*, Nat. Mater. **9**, 139 (2010)]. We underline the distinct features of magnetic and liquid-crystal torons and calculate phase diagrams indicating their stability regions.

DOI: 10.1103/PhysRevB.98.054404

I. INTRODUCTION

In magnetic compounds lacking inversion symmetry, the underlying crystal structure induces a specific asymmetric exchange coupling, the so-called Dzyaloshinskii-Moriya interaction (DMI) [1]. Within a continuum approximation for magnetic properties, the DMI is expressed by Lifshitz invariants (LI) involving first derivatives of the magnetization **m** with respect to the spatial coordinates,

$$\mathcal{L}_{i,j}^{(k)} = m_i \partial m_j/\partial x_k - m_j \partial m_i/\partial x_k, \tag{1}$$

and in a general case of cubic helimagnets has the following form [1,2]:

$$w_D = \mathcal{L}_{y,z}^{(x)} + \mathcal{L}_{x,z}^{(y)} + \mathcal{L}_{x,y}^{(z)} = \mathbf{m} \cdot \mathrm{rot}\mathbf{m}. \tag{2}$$

A variety of noncollinear magnetic states (e.g., one-dimensional helicoid and conical phases) is stabilized owing to this relativistic DMI.

LIs (1) also help to overcome the constraints of the Hobart-Derrick theorem [3] and yield countable particlelike topological excitations, chiral skyrmions [2,4–6]. Recently, skyrmion lattice states (SkLs) and isolated skyrmions (ISs) were discovered in bulk crystals of chiral magnets near the magnetic ordering temperatures [7–9] and in nanostructures with confined geometries over larger temperature regions [10–13].

The small size and easy manipulation of skyrmions by electric fields and currents [14–16] generated enormous interest in their applications in information storage and processing [17,18]. Furthermore, the complex three-dimensional internal structure of ISs and character of skyrmion-skyrmion interaction are imposed by a surrounding "parental" state, e.g., a state homogeneously magnetized along the field (repulsive inter-skyrmion potential) [19], a conical phase with the wave vector along the field (attraction) [20,21], or a tilted ferromagnetic state in magnets with polar crystal structure and easy-plane anisotropy (anisotropic potential) [22], which extends even further the skyrmion functionalities in prototype spintronic devices [21].

The twisting magnetization **m** in the skyrmions also matches boundary conditions at the confining surfaces of magnetic nanostructures. In particular in nanolayers of cubic helimagnets [23,24] with thickness L and free boundary conditions at the lower ($z = -L/2$) and upper surfaces [$z = L/2$; Fig. 1(a)], the structure of skyrmions is altered by additional chiral twists [23,24]. The skyrmion solutions at the surfaces are the result of the interplay between Lifshitz invariants $\mathcal{L}_{i,j}^{(x,y)}$, requiring skyrmion helicity $\gamma = \pi/2$, and $\mathcal{L}_{i,j}^{(z)}$, leading to the inward and outward rotational sense of the magnetization [see the structure of a Bloch-type skyrmion for $z = 0$ and $z = \pm L/2$ in Fig. 1(a)]. Thus, the skyrmion in thin layers of cubic helimagnets could be visualized as a composite object. The central part in the middle of the layer has higher (positive) magnetic energy than the conical phase (Fig. 1(b); see also Fig. 6(a) in Ref. [25]). However, the negative energy density in a narrow surface region associated with the additional twists may enable the lower total energy of skyrmions and thus lead to their thermodynamical stability.

Topological point defects (Bloch points [26,27]) may disrupt the smooth magnetization rotation and extend even further the variety of particlelike states in thin layers of cubic helimagnets. In particular due to the specific energetics exhibiting an excessive positive energy over the film thickness, isolated skyrmions may break and transform into a pair of chiral bobbers attached to the upper and the lower surfaces of the layer [Fig. 1(c)] [28]. Then, the structure of the bobbers is balanced by the negative energy contribution stemming from additional surface twists and the positive energy due to the point defect [Fig. 1(d)]. The Bloch point (BP) that terminates the structure of a bobber is situated at a finite distance from

*leonov@hiroshima-u.ac.jp

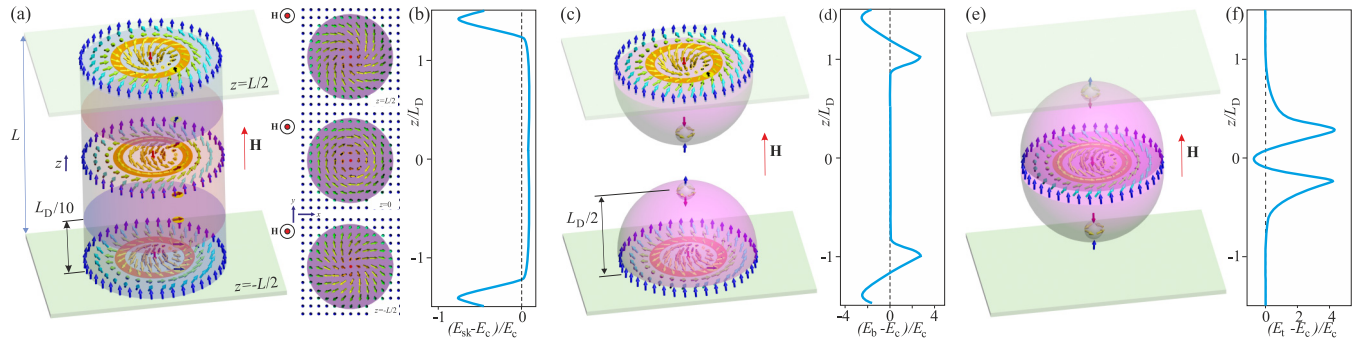

FIG. 1. Localized particlelike states in cubic thin-film helimagnets. (a) Skyrmionic defect-free filament surrounded by the field-polarized or conical phases. In thin layers of cubic helimagnets, the structure of a skyrmionic filament becomes additionally modulated in the near-surface region of width $L_D/10$. Snapshots in the transversal xy plane show the structure of skyrmions in the middle layer ($z = 0$, helicity value is $\pi/2$) and for two opposite surfaces with inward and outward changes in the azimuthal angle (helicity) of the magnetization. (c) Schematic representation of chiral bobbers, particlelike states localized near layer surfaces and culminating in two BPs. (e) Schematic representation of magnetic torons, spatially localized three-dimensional skyrmions composed of a skyrmion filament of finite length cupped by two BPs terminating its prolongation. (b), (d), and (f) The energy densities of skyrmions E_{sk}, bobbers E_b, and torons E_t averaged over the xy plane and computed with respect to the energy E_c of the conical phase for $h = 0.5$ in the model (3), respectively.

the surface [Fig. 1(c)] [28]. The chiral bobbers may provide an alternative approach for data encoding and thus may be used along with skyrmions in magnetic solid-state memory devices [29].

Interactions described by LIs (1) arise in other noncentrosymmetric condensed-matter systems (such as antiferromagnets, chiral liquid crystals, ferroelectrics, and multiferroics) and are also responsible for the formation of multidimensional solitonic states and spatially modulated phases in these materials. In chiral liquid crystals (LCs), a surprisingly large diversity of naturally occurring and laser-generated topologically nontrivial solitons with differently knotted nematic fields has been recently investigated [30–32]. In particular, a LC toron represents a localized particle consisting of two BPs at finite distance and a convex-shaped skyrmion stretching between them [Fig. 1(e)]. Due to the gradually varying skyrmion helicity, the energy density becomes negative in the toron's cross section, which is balanced by the positive-energy contributions from two BPs [Fig. 1(f)]. Thus, such a particle utilizes energetically favorable additional twists and simultaneously satisfies the boundary conditions at the confining substrates with strong surface anchoring [33,34]. Recently, a low-voltage-driven motion of such topological LC defects with precise control of both the direction and speed was realized in nematic fluids [33], which can be considered a LC counterpart of the racetrack memory suggested for magnetic skyrmions.

In the present paper, we pose a problem of skyrmion nucleation in thin layers of cubic helimagnets, occurring via elongation of torons (homogeneous nucleation) and chiral bobbers (heterogeneous nucleation) since these entities are claimed to have lower activation energy than ISs. Since the potential barrier that must be overcome for a particle to appear is a function of the interfacial energy with respect to the surrounding conical or homogeneous state, the heterogeneous nucleation is more common than the homogeneous one. In particular in Ref. [28], the spontaneous nucleation of magnetic bobbers has been observed during the simulated temperature annealing with no appearing magnetic torons. The LC torons, however, are easily laser generated, as described in Ref. [31]: (i) the realignment of the LC director $\mathbf{n}$ was locally achieved by coupling it to the optical-frequency electric field of the laser beam; (ii) alternatively, the chiral nematic LC was locally heated to the isotropic phase of the material by a focused laser beam, so that the spontaneous appearance of torons could then be prompted upon quenching it back to the LC phase.

We demonstrate that torons and bobbers are solutions of the equations describing the equilibrium states of a noncentrosymmetric system and can exist as metastable states in the saturated and modulated phases. We argue, however, that in the isotropic case (3) both types of skyrmion nucleation are not feasible. To facilitate elongation of torons and bobbers and their subsequent transformation into the ordinary ISs that pierce the layer, we apply uniaxial anisotropy as the primary candidate making the skyrmion core negative with respect to the surrounding state. We also construct the phase diagram of solutions indicating the stability limits of torons and elucidate their physical nature.

II. THE MODEL

A. A continuum energy functional

The standard model for magnetic states in cubic noncentrosymmetric ferromagnets is based on the energy density functional [1,35]

$$w = A\,(\mathbf{grad}\,\mathbf{m})^2 + D\,\mathbf{m}\cdot\mathrm{rot}\,\mathbf{m} - \mu_0\,M\mathbf{m}\cdot\mathbf{H}, \qquad (3)$$

including the principal interactions essential to stabilize modulated states: the exchange stiffness with constant A, Dzyaloshinskii-Moriya coupling energy with constant D, and the Zeeman energy; $\mathbf{m} = (\sin\theta\cos\psi; \sin\theta\sin\psi; \cos\theta)$ is the unity vector along the magnetization vector $\mathbf{M} = \mathbf{m}M$, and $\mathbf{H}$ is the applied magnetic field along the z axis. The film is infinite in the x and y directions; that is, we exclude any influence of the lateral sample boundaries on the nucleation process since inhomogeneities near sample edges readily provide nucleation centers for skyrmions (see, e.g., Fig. 3 in Ref. [36] or Fig. 3 in Ref. [37] showing half skyrmions at the lateral edges, which

can be considered two-dimensional defect-free counterparts of chiral bobbers [28]). We also neglect the influence of dipole-dipole interactions. The influence of dipole-dipole interaction on the nucleation processes of torons and bobbers will be considered elsewhere.

B. A classical spin model

To investigate the solutions for magnetic torons, we also use the discretized version of Eq. (3):

$$w = J\sum_{\langle i,j\rangle}(\mathbf{S}_i\cdot\mathbf{S}_j) - \sum_i \mathbf{H}\cdot\mathbf{S}_i - K_u S_z^2 - D\sum_i(\mathbf{S}_i\times\mathbf{S}_{i+\hat{x}}\cdot\hat{x} + \mathbf{S}_i\times\mathbf{S}_{i+\hat{y}}\cdot\hat{y} + \mathbf{S}_i\times\mathbf{S}_{i+\hat{z}}\cdot\hat{z}). \quad (4)$$

The classical spins of the unit length are placed in the knots of a three-dimensional cubic lattice. Here, $\langle i, j\rangle$ denotes pairs of nearest-neighbor spins. The first term describes the ferromagnetic nearest-neighbor exchange with $J < 0$ (in the numerical simulation $J = -1$ is used). The Dzyaloshinskii-Moriya constant D defines the period of modulated structures p via the following relation: $D/J = \tan(2\pi/p)$ [thus, we use the discretized version of the DMI (2) in our forthcoming simulations]. Or vice versa, one chooses the period of the modulations p (a discrete analog of L_D) for the computing procedures and defines the corresponding value of the DMI constant. In what follows, the Dzyaloshinskii-Moriya constant is set to 0.48, which corresponds to one-dimensional modulations with a period of 14 lattice spacings in a zero field (for further details on the methods see Refs. [20,37]). The size of our numerical grid is set to $100 \times 100 \times L$, which is large enough to accommodate an IS within the conical phase and to take into account all the subtleties of its internal structure.

C. Energy minimization and numerical solutions for torons and bobbers

The solutions for particlelike states in the film (Fig. 1) are derived by the Euler equations for energy functional (3) together with the Maxwell equations and with corresponding boundary conditions. The solutions depend on the two control parameters of the model (3), the *confinement ratio*, $\nu = L/L_D$, and the reduced value of the applied magnetic field, $h = H/H_D$, where $L_D = 4\pi A/|D|$ is the *helix period* and $\mu_0 H_D = D^2/(2AM)$ is the *saturation field* [4,35].

Metastable torons were initially prepared from two chiral bobbers (obtained with a relatively high kinetic cycle temperature T_k within the saturated state). Further, the toron structure was refined using either the iterative simulated annealing procedure (with a relatively low kinetic cycle temperature T_k) or a single-step Monte Carlo dynamics with the Metropolis algorithm (for details, see Sec. II B in Ref. [38]). Alternatively, solutions for torons and bobbers were obtained with the Landau-Lifshitz-Gilbert (LLG) equation starting from the initial ansatz solutions and further using the fourth-order Runge-Kutta method and a dimensionless damping parameter $\alpha = 0.1$ (for details see the Method section of Ref. [39]). Then, the dynamic process of toron elongation and the complex three-dimensional (3D) structure of magnetic torons with different lengths along z were checked at fixed time intervals of the LLG equation [39] or after the fixed number of steps in the Metropolis algorithm [38].

III. THE PROPERTIES AND 3D TOPOLOGY OF MAGNETIC TORONS

The 3D structure of magnetic torons is stipulated by the tendency to build into the conical phase [Fig. 2(a)]. By this process, the magnetic torons develop a lateral transitional region towards the cones (the so-called shell [20,21]) and terminate their structure along z by two BPs. Three different composite sections along the z axis can be singled out in a magnetic toron:

(1) *The core section* is a central part of a magnetic toron. Figure 2(b) shows the structure of this part in the xy plane: the central circular region nearly preserves the axial symmetry, whereas the transient region with the asymmetric crescent-like shape is formed with respect to the embedding conical state. This asymmetric profile of the cross section forms a screwlike modulation along the z axis trying to match the conical phase at each coordinate z.

The inherent properties of such nonaxisymmetric skyrmion solutions with infinite length have been extensively studied in Refs. [20,21,40]. It was shown that the shell has positive energy with respect to the cone phase and thus underlies an attractive interskyrmion potential.

In the present case of magnetic torons, the core section extends along z over a finite length. This implies that the shell, which is obtained with the energy averaging along z, has different magnitudes depending on the azimuthal angle. In Fig. 2(g), we show the energy density (3) after integration with respect to the z coordinate,

$$e(x, y) = (1/l)\int_l w dz. \quad (5)$$

For this integration procedure we used a magnetic toron with length $l = p/2$ of its core section. Such an energy distribution underlies an anisotropic but still attracting skyrmion-skyrmion interaction. Figure 2(h) shows a horizontal line scan across $e(x, y)$: it has a bump with positive energy density from the left which is essentially lowered on the right side.

Figure 2(e) shows the energy density $\epsilon(z)$ averaged over the xy plane as a function of the z coordinate. The core section of a magnetic toron is marked by the red shading.

(2) The second is the section of magnetic torons with *additional twists*. Figure 2(c) shows the structure of this part in the xy plane. The magnetization in this section does not retain its helicity equaling $\pi/2$ as in the core section, but rather undergoes an additional in-plane rotation while propagating along z. The sense of the magnetization rotation is opposite while moving towards upper and lower BPs; that is, the magnetization undergoes an outward (with the helicity decreasing towards zero) and/or inward rotation (with the helicity increasing towards π [24,25]). Due to the rotational DMI terms (2) along z, the additional negative energy (with the value larger than in the core section) can be "earned." In Fig. 2(e) this region has orange shading. The color plot in Fig. 2(c) displays the spin structure for the fixed value of the z

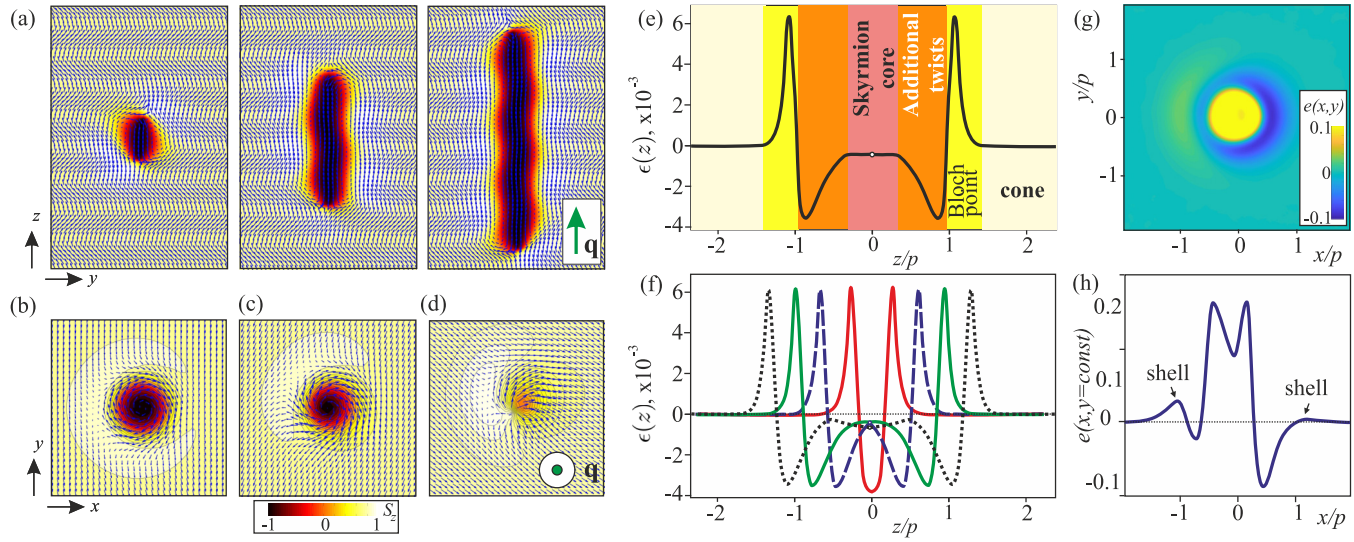

FIG. 2. (a) Magnetic structure of isolated magnetic torons with different lengths along the z axis and surrounded by the conical phase. The color plots indicate the z component of the magnetization; blue arrows are projections of the magnetization onto the yz plane. The green arrow shows the $\mathbf{q}$ vector of the conical phase. (b)–(d) Composite parts of the magnetic torons shown in the transversal xy plane: (b) the core section, (c) the section with the additional twists along z, and (d) the Bloch point (see text for details). The color indicates the z component of the magnetization, whereas the blue arrows are the projections of the magnetization onto the xy plane. (e) The energy density $\epsilon(z)$ averaged over the xy plane and computed with respect to the conical phase shows the negative energy density in the region of additional twists (orange shading) and the core region (red shading) balanced by the positive energy associated with BPs (yellow region). (f) In magnetic torons with longer extension along z, the negative energy density $\epsilon(z)$ is gained owing to the core region. (g) The color plot for the energy density $e(x, y)$ obtained from (5) and computed with respect to the energy of the conical phase. A magnetic toron with core section length $p/2$ was chosen for simplicity. Such an asymmetric energy distribution implies anisotropic attracting skyrmion-skyrmion interaction. (h) The horizontal line scan of $e(x, y)$ compares the magnitudes of the shell from the left and right sides of the core section.

coordinate corresponding to the minimal energy density in the orange shaded region.

(3) *The Bloch points* represent singular points at which the smooth rotation of the magnetization is disrupted [26,27]. The structure of the Bloch points is shown in Fig. 2(d) in the xy plane. The corresponding section of the magnetic torons is marked by the yellow shading in Fig. 2(e). The z coordinate of the color plot corresponds to the maximal energy value in Fig. 2(e).

Thus, the magnetic toron can be visualized as a composite object formed by a finite-length section of the nonaxisymmetric skyrmions within the conical phase with the "attached" chiral bobbers at its ends.

IV. PHASE DIAGRAMS AND HOMOGENEOUS NUCLEATION

A. Skyrmion stabilization in thin films of cubic helimagnets due to the surface twists

The phase diagram of states constructed in Refs. [24,41] for a thin layer within model (3) shows vast areas of SkLs and spirals stabilized due to the additional surface twists and separated by the lines of the first-order phase transition from the conical phase (see inset of Fig. 3). ISs within the conical phase, however, are metastable particles for all values of the confinement ratio [28] (except the small orange shaded region for $\nu < 1$ in which the energy of an IS becomes negative). The reason lies in the specific transient region between an IS and the conical phase (dubbed "shell" in Ref. [20]) that bears the positive energy density and increases linearly with the thickness. Moreover, the additional surface twist (and hence the associated negative energy) is essentially reduced in the IS compared with the SkL [28]. The energy of chiral bobbers, on the contrary, is only field dependent and does not depend on the layer thickness [28], which makes bobbers the lowest-energy metastable states and precludes the process of heterogeneous skyrmion nucleation. The homogeneous nucleation of skyrmions is also prevented within the model (3) since the part of the skyrmion with the positive energy density must be implanted into the toron's structure, which

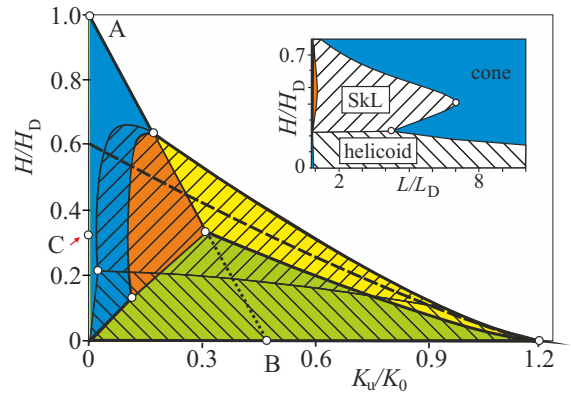

FIG. 3. Diagram in coordinates H/H_D-K_u/K_0 reflecting the internal properties of magnetic torons (see the text for details). The inset shows the phase diagram for model (3) with $K_u = 0$.

necessarily increases its energy. In particular in Ref. [42] it was shown that LC torons exist in some range of the confinement ratio. If the confinement ratio is too small, the anchoring force necessitates the toron transformation into the aligned state. On the contrary, if one tries to elongate the LC torons by increasing the confinement ratio, the torons undergo an elliptical instability towards the more stable fingerprint texture.

B. Skyrmion stabilization due to the uniaxial anisotropy

In the following, we supply the model (3) with a uniaxial anisotropy of the easy-axis type [43] with the easy axis **a** coaligned with the field **H**, $w_{an} = -K_u(\mathbf{m}\cdot\mathbf{a})^2$. $K_u > 0$ since for $K_u < 0$ the conical phase is the global minimum in the whole region of the phase diagram [44,45]. As a solution with period L_D, the conical phase exists below the critical field $H_C = H_D(1 - K_u/K_0)$, where $K_0 = D^2/(4A)$. The equilibrium parameters for this cone phase are expressed in the analytical form [35] as

$$\theta_c = \arccos(H/H_C),\ \psi_c = 2\pi z/L_D. \tag{6}$$

Above the critical field H_C, the cone phase transforms into the saturated state with $\theta = 0$ (straight line A-B in Fig. 3).

The diagram in Fig. 3 exhibits the following regions for magnetic torons. In the orange shaded region, the energy of the core section becomes negative with respect to the surrounding conical phase. Then, the magnetic toron undergoes an elongation: the longer the distance is between two Bloch points, the larger the amount of negative energy with respect to the conical phase "accumulates" in the core section. Moreover, the Bloch points might be expelled altogether at the sample surfaces, thus making the skyrmion even more energetically favorable. In the blue shaded region, the energy density of the core section in the magnetic torons is positive with respect to the conical phase, which disables their elongation. In the yellow shaded region, the magnetic torons have negative energy in their cores, but with respect to the surrounding homogeneous state: thus, the same process of skyrmion elongation might take place. The hatched regions display the thermodynamically stable hexagonal SkLs and helicoids and, owing to the first-order phase transition between different modulated phases, do not coincide with the colored regions for isolated torons. Hence, in the green shaded region of the phase diagram, torons undergo an elliptical instability with respect to the thermodynamically stable helicoid.

C. Magnetic torons and the *A*-phase phenomenon in cubic helimagnets near the ordering temperatures

A process of homogeneous skyrmion nucleation from magnetic torons must also be inherent in bulk cubic helimagnets. We treat the magnetic torons as nuclei of the first-order phase transition from the conical phase into the skyrmion lattice which may become paramount within A phases of bulk cubic helimagnets near the ordering temperature (e.g., in B20 magnets MnSi [7] and FeGe [8]). This transition may occur via formation of magnetic torons of finite length accompanied by their elongation (e.g., due to the cubic or exchange anisotropy, which also may lead to the negative energy density of skyrmion cores) and mutual attraction. We stress that a softened version

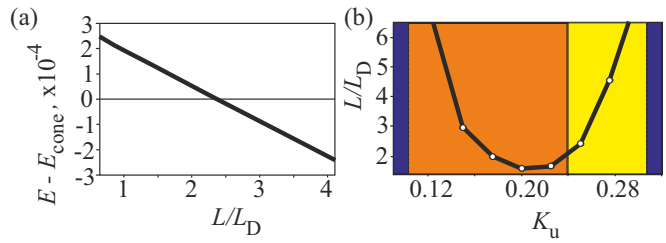

FIG. 4. (a) The total energy of a magnetic toron E_t for the fixed field and the anisotropy values, $H/H_0 = 0.5$, $K_u/K_0 = 0.25$, plotted as a function of the toron's length along z. The total energy becomes negative for some critical length l_{cr}. (b) The critical anisotropy-dependent length of magnetic torons l_{cr} for a fixed field value $H/H_0 = 0.5$ according to the phase diagram in Fig. 3. The orange and yellow shading was added to distinguish between torons within the conical and saturated states, respectively.

of the order parameter (magnetization) allows us to replace the notion of localized defects as BPs with smooth, but more complex, geometrical adaptation of ordering with regions of suppressed order-parameter intensity [46]. In particular, such a method was applied to construct a new modulated phase in bulk cubic helimagnets, a square lattice of half skyrmions [46], that does not exist with a fixed value of the order parameter.

V. TORON'S LONGITUDINAL STABILITY

Figure 2(f) highlights the tendency of magnetic torons to elongate: it shows the averaged energy density along z for magnetic torons with different longitudinal extensions. The critical length of a magnetic toron l_{cr}, which ensures the total negative energy (i.e., the sum of the energy of all three composite sections) with respect to the cone, varies throughout the orange shaded region of Fig. 3. The method to define the critical length l_{cr} is as follows: we define the energy E_t of magnetic torons with different lengths l for fixed parameters K_u and H [Fig. 4(b)]. We consider the length l of a magnetic toron to be the distance between two BPs [the distance between points with the maximal energy density in Fig. 2(e)]. Then, $E_t = 0$ with respect to the energy of the conical phase specifies the critical length l_{cr}. Figure 4(b) shows such a critical length l_{cr} as a function of K_u for a fixed value of the field $H/H_0 = 0.5$. The critical length $l_{cr}(K_u)$ of a magnetic toron reaches the minimal value in the middle of the orange shaded region and equals $1.65p$ for $K_u/K_0 = 0.2$. At the boundaries of the orange and yellow shaded regions, the critical length diverges to infinity: such torons lose their BPs, and consequently, the section with the additional twists transforms into the isolated nonaxisymmetric skyrmions studied in Refs. [20,21,40] and depicted in Fig. 1(a).

The internal structure of magnetic torons in the yellow region of the phase diagram (Fig. 3) is depicted in Fig. 5 and basically reproduces the structure of torons within the conical phase (Fig. 2); that is, three composite sections may be introduced as well [Figs. 5(c)–5(e)]. The crucial difference, however, lies in the absence of the shell since such magnetic torons laterally match the homogeneous background. Therefore, the skyrmions rather repulse each other (for details see Ref. [19]). At the boundary of the yellow shaded region (Fig. 3) the energy of an isolated skyrmion [which, according

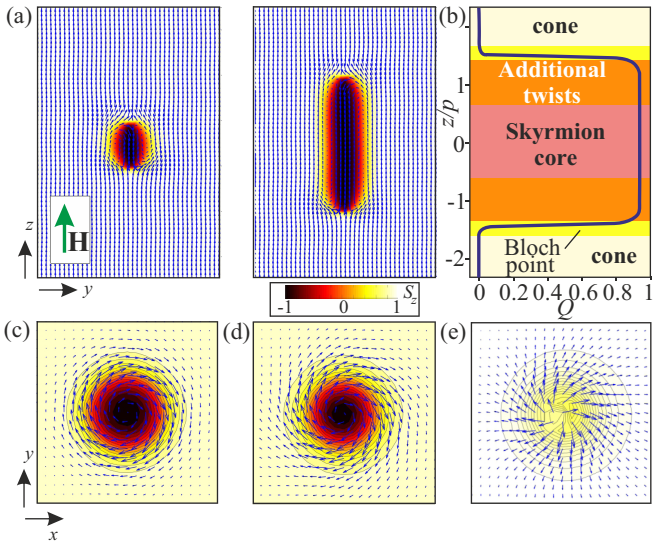

FIG. 5. (a) Magnetic structure of isolated magnetic torons with different lengths along the z axis and surrounded by the saturated phase. The color plot indicates the z component of the magnetization; blue arrows are projections of the magnetization onto the yz plane. (b) Topological charge Q (7) calculated in xy planes as a function of the z coordinate. The color shading corresponds to the color scheme in Fig. 2(e). (c)–(e) Composite parts of a magnetic toron shown in the transversal xy plane: (c) the core region, (d) the region with the additional twists along z, (e) the Bloch point (see the text for details). The color indicates the z component of the magnetization, whereas the blue arrows are the projections of the magnetization onto the xy plane.

to Fig. 4(b), has an infinite length] becomes zero with respect to the homogeneous state: below this line, the skyrmions may condense into a thermodynamically stable skyrmion lattice (hatched region), whereas above they exist as metastable excitations. Thus, this upper boundary is the line of the second-order phase transition between the skyrmion lattice and the homogeneous state [4,19]. Figure 5(b) shows the topological charge Q along the z axis:

$$Q = \frac{1}{4\pi} \iint d^2 r \mathbf{m} \frac{\partial \mathbf{m}}{\partial x} \frac{\partial \mathbf{m}}{\partial y}. \tag{7}$$

It equals 1 in the core regions and the region of additional twists (red and orange shading) and decreases to 0 in the section with BPs (yellow shading).

The stable SkL with the hexagonal arrangement of skyrmions exists in the hatched region of Fig. 4(a). The line of the first-order phase transition between the skyrmion lattice and the conical phase does not coincide with the line at which the energy of an isolated magnetic toron becomes negative. The reason lies in the skyrmion shell with positive energy. For the same reason, the first-order phase transition, which occurs between cones and SkLs and involves the formation of transient regions with positive energy between corresponding phase domains, will lag until the linear energy density of the transient region is balanced by the negative surface energy density of a new phase with respect to the old one. In Ref. [40] in particular, it was observed experimentally that the skyrmion clusters within the conical phase have the tendency to merge

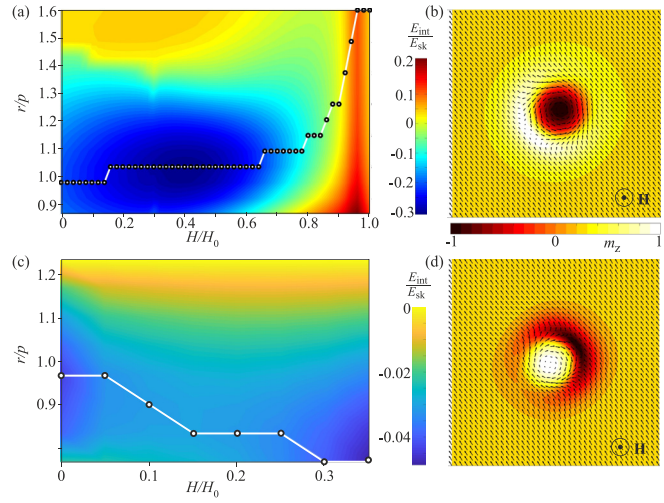

FIG. 6. (a) and (c) reduced energy of the interaction between two nonaxisymmetric skyrmion filaments surrounded by the conical phase, $E_{\rm int}/E_{sk}$, shown as a color plot in coordinates of r (the distance between the skyrmion centers) and the applied magnetic field H/H_0 ($K_u = 0$). The attraction between skyrmions of (b) negative and (d) positive polarities has been considered.

into one bigger cluster: they diminish the energy of the domain boundary with the conical phase by decreasing its linear energy density.

VI. SKYRMION-SKYRMION ATTRACTION

In Fig. 6, we plot the interaction energy between two nonaxisymmetric skyrmions $E_{\rm int}/E_{sk}$ (in units of the total equilibrium energy of an isolated asymmetric skyrmion E_{sk}) as a function of the distance between the skyrmion centers r calculated for different values of the applied field ($K_u = 0$). It is seen that the largest interaction energy is achieved at $H/H_D = 0.4$ and equals $\sim 0.3 E_{sk}$. In Ref. [44] (see their Fig. 10), it was shown that in the field $H/H_D = 0.4$ the difference between the energy densities of the hexagonal SkL and the cone phase is minimal. Thus, it was suggested that the SkL could be stabilized with respect to the cones by additional anisotropic energy contributions exactly around this field value. With our insight, we may add that the energy of the shell in ISs is the largest for this field value. Therefore, while condensing into the lattice and thus eliminating the shell, the skyrmions acquire the largest increase in their energy density.

Note that the conical phase accommodates two types of ISs with magnetization in their cores, either along or opposite the field. At zero field, two states with opposite polarities share the same energy (note the opposite location of the crescent-shaped region in two types of ISs with respect to their circular cores). In an applied magnetic field, however, the skyrmions with the positive polarity may exist only in a narrow field interval (for $K_u = 0$ the range is 0–C in Fig. 3).

VII. HETEROGENEOUS NUCLEATION

Transition from the chiral bobbers [Fig. 7(a)] to IS [Fig. 7(d)] occurs via an intermediate state [Fig. 7(b)] with two Bloch points located at a fixed distance from each other. In

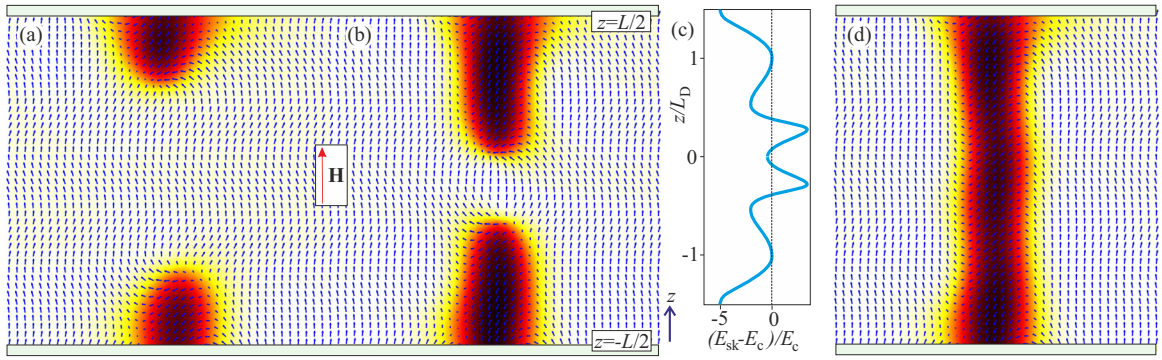

FIG. 7. Heterogeneous nucleation of defect-free skyrmions (d) from chiral bobbers with defects (a) occurring via an intermediate state (b). (c) The energy density of such an intermediate state averaged over the xy plane and computed with respect to the energy E_c of the conical phase for $H/H_D = 0.5$, $K_u/K_0 = 0.25$ in model (3).

this case, the energy distribution in the region between two BPs [Fig. 7(c)] looks qualitatively the same as for a toron [Fig. 1(f)] and is stipulated by the additional twist of the magnetization which necessarily accompanies a chiral Bloch point. Thus, some potential barrier must be overcome to annihilate a pair of BPs, which becomes also inherent for bulk helimagnets filled with torons of finite length. Hence, we anticipate small jumps of the magnetization associated with this process in A phases of bulk cubic helimagnets, reminiscent of the magnetic Barkhausen effect.

VIII. TORONS IN CHIRAL NEMATICS

A. The free Frank energy

Within the continuum theory the equilibrium distributions of the director $\mathbf{n}(\mathbf{r})$ in confined liquid crystals are derived by solving the Euler equations for the Frank free energy density functional [47,48]

$$f(\mathbf{n}) = \frac{K_1}{2}(\mathrm{div}\,\mathbf{n})^2 + \frac{K_2}{2}(\mathbf{n}\cdot\mathrm{rot}\,\mathbf{n} - \mathrm{q}_0)^2 + \frac{K_3}{2}(\mathbf{n}\times\mathrm{rot}\,\mathbf{n})^2 - \frac{\varepsilon_a}{2}(\mathbf{n}\cdot\mathbf{E})^2 - \frac{\chi_a}{2}(\mathbf{n}\cdot\mathbf{H})^2. \quad (8)$$

Here, K_i $(i = 1, 2, 3)$ and q_0 are elastic constants; $\mathbf{E}$ and $\mathbf{H}$ are the vectors of applied electric and magnetic fields, and ε_a and χ_a are values of dielectric and diamagnetic anisotropies. In the following for the sake of simplicity we will consider only effects imposed by the magnetic field and restrict our analysis to the one-constant approximation ($K_1 = K_2 = K_3 = K$). In this case the energy (8) is reduced to the following expression:

$$f_v = \frac{K}{2}(\mathrm{grad}\,\mathbf{n})^2 + Kq_0\mathbf{n}\cdot\mathrm{rot}\,\mathbf{n} - \frac{\chi_a}{2}(\mathbf{n}\cdot\mathbf{H})^2. \quad (9)$$

We use here the equation $(\mathrm{grad}\,\mathbf{n})^2 = (\mathrm{div}\,\mathbf{n})^2 + (\mathbf{n}\cdot\mathrm{rot}\,\mathbf{n})^2 + (\mathbf{n}\times\mathrm{rot}\,\mathbf{n})^2 + \langle\text{surface terms}\rangle$, which holds for any unity vector $\mathbf{n}$ (for details see, e.g., Ref. [49]).

Equation (9) implies close relations between chiral textures in both condensed-matter systems, in chiral magnets and liquid crystals. However, in contrast to magnetic systems still favoring smooth distributions of the order parameter, liquid crystals usually form patterns composed of various types of singularities. Defects in liquid crystals are of various dimensionalities, not only point defects but also the line and walls, and appear due to the prevalence of orientational order over positional order in the applied magnetic or electric fields [47]. Control and understanding of the nature of topological defects in LCs are currently a topic of utmost interest, as the topological defects transfer topological singularities to light and could be exploited in novel devices based on singular photonics [42]. In the defects the director $\mathbf{n}$ is said to be well defined [42,50] and the properties of defects are well controlled. These results for observations of specific skyrmion states with defects in confined cholesteric systems can help us to investigate similar structures in chiral magnets. Liquid crystals have several advantages over magnetic systems for the investigation of various inhomogeneous structures. The system parameters can be varied over wide limits to establish the necessary conditions for a given experiment; as a rule experiments are conducted at room temperature and are comparatively simple; the results of investigations are easily visualized [31,51], to a degree not usually attainable in the investigation of magnetic systems.

B. Comparison of magnetic and LC torons

The absence of a Zeeman-like term in the elastic (Frank) free energy [47,48] (9) leads to the inability of LC torons to elongate, as described for their magnetic counterpart in Fig. 2. The reason is that the core section of LC torons obtained within the model (9) has positive energy compared with the surrounding phase (see, e.g., Ref. [43], which showed that in bulk cubic helimagnets the SkL is stabilized by the simultaneous effect of the magnetic field and the easy-axis anisotropy). Therefore, a LC toron can be visualized as two chiral bobbers attached together by the squeezed core section. The helicity of the director continuously changes when going from one Bloch point to another and has a value of $\pi/2$ in the central plane. The magnetic counterpart of such LC torons exists in the white region of the phase diagram in Fig. 3. Reference [50] showed, however, that the BPs comprising such LC torons do not annihilate and are bound to each other at a certain well-defined distance. Thus, a certain potential barrier is associated with the creation and annihilation of torons.

According to the phase diagram in Fig. 3, without a Zeeman term in (3) one gets solutions for LC torons for $K_u/K_0 > 1.24$, i.e., the case of strong anchoring. For a weaker anchoring, one may enter the region of the spiral thermodynamical stability

(hatched region in Fig. 3). In this case, the defect-free localized solutions, spherulites [52], may occur; such solutions, however, may undergo an elliptical instability towards spirals.

Interestingly, the LC torons with the nonaxisymmetric core section [realized in Fig. 2(b) in the applied magnetic field] may be realized as a result of the competition between the surface anchoring and the electric-field term in (8): whereas the surface anchoring tends to orient the director $\mathbf{n}(\mathbf{r})$ perpendicular to the confining glass plates, the electric field $\mathbf{E}$ with the negative dielectric anisotropy ε_a is parallel to them (see in particular Fig. 1 in Ref. [33]). As a result of such an interplay, one creates an analog of the conical phase around a skyrmion that induces an attractive toron-toron interaction and experimentally observed toron chains [34]. Moreover, the directional motion of such skyrmions is possible as a response to modulated electric fields: when alternating current with some frequency is applied to a confined skyrmion with the axisymmetric structure [Fig. 5(c)], it transforms into a nonaxisymmetric solution [Fig. 2(b)] back and forth, thus inducing a squirming motion.

In general in chiral nematic LCs, point and line defects spontaneously occur as a result of symmetry-breaking phase transitions, and versatile 3D topological solitons might be stabilized. As an alternative to SkLs, different ordered structures of defects could be organized. Reference [50] showed that using a scanning laser generation system, one can program a focused laser beam to generate periodic lattices formed by the metastable LC torons. In chiral magnets, different periodic arrangements of BPs have also been considered. In particular, the monopole-antimonopole pairs were arranged in the form of a lattice in which they are connected by the skyrmion strings [53]. It was shown that such a lattice has nontrivial transport properties which may result, in particular, in a novel magnetoresistivity effect as applied for MnGe [53].

IX. CONCLUSIONS

To conclude, we have derived numerical solutions for torons in the saturated and cone phases of cubic helimagnets. Along with the chiral bobbers introduced in Ref. [28], magnetic torons may serve as nuclei of skyrmion matter: the energy of a magnetic toron may become negative in some region of the constructed phase diagrams (Fig. 3), thus instigating its elongation. Subsequently, defect-free ISs (or torons and bobbers of finite length) due to the mutual lateral attraction form clusters and eventually an ideal SkL. Such a process follows the definition of a nucleation-type phase transition introduced by de Gennes [54] for (continuous) transitions into incommensurate modulated phases. A comparison of magnetic torons with their LC counterparts will facilitate their experimental investigation in thin-layer and bulk chiral helimagnets.

ACKNOWLEDGMENTS

The authors are grateful to I. Smalyukh and A. Bogdanov for useful discussions. This work was funded by the JSPS Core-to-Core Program, Advanced Research Networks (Japan), and a JSPS Grant-in-Aid for Research Activity Start-up 17H06889. A.O.L. thanks U. Nitzsche for technical assistance.

[1] I. E. Dzyaloshinskii, Zh. Eksp. Teor. Fiz. **46**, 1420 (1964) [Sov. Phys. JETP **19**, 960 (1964)].
[2] A. N. Bogdanov and D. A. Yablonskii, Zh. Eksp. Teor. Fiz. **95**, 178 (1989) [Sov. Phys. JETP **68**, 101 (1989)].
[3] R. Rajaraman, *Solitons and Instantons: An Introduction to Solitons and Instantons in Quantum Field Theory* (North-Holland, Amsterdam, 1982).
[4] A. Bogdanov and A. Hubert, J. Magn. Magn. Mater. **138**, 255 (1994); **195**, 182 (1999).
[5] N. Nagaosa and Y. Tokura, Nat. Nanotechnol. **8**, 899 (2013).
[6] U. K. Rößler, A. A. Leonov, and A. N. Bogdanov, J. Phys.: Conf. Ser. **303**, 012105 (2011).
[7] S. Mühlbauer, B. Binz, F. Jonietz, C. Pfleiderer, A. Rosch, A. Neubauer, R. Georgii, and P. Böni, Science **323**, 915 (2009).
[8] H. Wilhelm, M. Baenitz, M. Schmidt, U. K. Rößler, A. A. Leonov, and A. N. Bogdanov, Phys. Rev. Lett. **107**, 127203 (2011).
[9] I. Kezsmarki, S. Bordacs, P. Milde, E. Neuber, L. M. Eng, J. S. White, H. M. Ronnow, C. D. Dewhurst, M. Mochizuki, K. Yanai, H. Nakamura, D. Ehlers, V. Tsurkan, and A. Loidl, Nat. Mater. **14**, 1116 (2015).
[10] X. Z. Yu, Y. Onose, N. Kanazawa, J. H. Park, J. H. Han, Y. Matsui, N. Nagaosa, and Y. Tokura, Nature (London) **465**, 901 (2010).
[11] X. Z. Yu, N. Kanazawa, Y. Onose, K. Kimoto, W. Z. Zhang, S. Ishiwata, Y. Matsui, and Y. Tokura, Nat. Mater. **10**, 106 (2011).
[12] H. Du, D. Liang, C. Jin, L. Kong, M. J. Stolt, W. Ning, J. Yang, Y. Xing, J. Wang, R. Che, J. Zang, S. Jin, Y. Zhang, and M. Tian, Nat. Commun. **6**, 7637 (2015).
[13] D. Liang, J. P. DeGrave, M. J. Stolt, Y. Tokura, and S. Jin, Nat. Commun. **6**, 8217 (2015).
[14] T. Schulz, R. Ritz, A. Bauer, M. Halder, M. Wagner, C. Franz, C. Pfleiderer, K. Everschor, M. Garst, and A. Rosch, Nat. Phys. **8**, 301 (2012).
[15] F. Jonietz, S. Mühlbauer, C. Pfleiderer, A. Neubauer, W. Münzer, A. Bauer, T. Adams, R. Georgii, P. Böni, R. A. Duine, K. Everschor, M. Garst, and A. Rosch, Science **330**, 1648 (2010).
[16] P.-J. Hsu, A. Kubetzka, A. Finco, N. Romming, K. von Bergmann, and R. Wiesendanger, Nat. Nanotechnol. **12**, 123 (2017).
[17] J. Sampaio, V. Cros, S. Rohart, A. Thiaville, and A. Fert, Nat. Nanotechnol. **8**, 839844 (2013).
[18] E. M. R. Tomasello, R. Zivieri, L. Torres, M. Carpentieri, and G. Finocchio, Sci. Rep. **4**, 6784 (2014).
[19] A. O. Leonov, T. L. Monchesky, N. Romming, A. Kubetzka, A. N. Bogdanov, and R. Wiesendanger, New J. Phys. **18**, 065003 (2016).
[20] A. O. Leonov, T. L. Monchesky, J. C. Loudon, and A. N. Bogdanov, J. Phys.: Condens. Matter. **28**, 35LT01 (2016).
[21] A. O. Leonov, J. C. Loudon, and A. N. Bogdanov, Appl. Phys. Lett. **109**, 172404 (2016).
[22] A. O. Leonov and I. Kezsmarki, Phys. Rev. B **96**, 014423 (2017).

[23] F. N. Rybakov, A. B. Borisov, and A. N. Bogdanov, Phys. Rev. B **87**, 094424 (2013).
[24] A. O. Leonov, Y. Togawa, T. L. Monchesky, A. N. Bogdanov *et al.*, Phys. Rev. Lett. **117**, 087202 (2016).
[25] D. McGrouther, R. J. Lamb, M. Krajnak, S. McFadzean, S. McVitie, R. L. Stamps, A. O. Leonov, A. N. Bogdanov, and Y. Togawa, New J. Phys. **18**, 095004 (2016).
[26] A. P. Malozemoff and J. C. Slonczewski, *Magnetic Domain Walls in Bubble Materials* (Academic Press, New York, 1979).
[27] A. Thiaville, J. M. Garcia, R. Dittrich, J. Miltat, and T. Schrefl, Phys. Rev. B **67**, 094410 (2003).
[28] F. N. Rybakov, A. B. Borisov, S. Blügel, and N. S. Kiselev, Phys. Rev. Lett. **115**, 117201 (2015).
[29] F. Zheng, F. N. Rybakov, A. B. Borisov, D. Song, S. Wang, Z.-A. Li, H. Du, N. S. Kiselev, J. Caron, A. Kovács, M. Tian, Y. Zhang, S. Blüugel, and R. E. Dunin-Borkowski, Nat. Nanotechnol. **13**, 451 (2018).
[30] I. I. Smalyukh, Y. Lansac, N. Clark, and R. Trivedi, Nat. Mater. **9**, 139 (2010).
[31] P. J. Ackerman and I. I. Smalyukh, Phys. Rev. X **7**, 011006 (2017).
[32] P. J. Ackerman and I. I. Smalyukh, Nat. Mater. **16**, 426 (2016).
[33] P. J. Ackerman, T. Boyle, and I. I. Smalyukh, Nat. Commun. **8**, 673 (2017).
[34] P. J. Ackerman, J. van de Lagemaat, and I. I. Smalyukh, Nat. Commun. **6**, 6012 (2015).
[35] P. Bak and M. H. Jensen, J. Phys. C **13**, L881 (1980).
[36] J. Iwasaki, M. Mochizuki, and N. Nagaosa, Nat. Nanotechnol. **8**, 742 (2013).
[37] R. Keesman, A. O. Leonov, P. van Dieten, S. Buhrandt, G. T. Barkema, L. Fritz, and R. A. Duine, Phys. Rev. B **92**, 134405 (2015).
[38] A. O. Leonov and I. Kezsmarki, Phys. Rev. B **96**, 214413 (2017).
[39] A. Leonov and M. Mostovoy, Nat. Commun. **6**, 8275 (2015).
[40] J. C. Loudon, A. O. Leonov, A. N. Bogdanov, M. Ciomaga Hatnean, and G. Balakrishnan, Phys. Rev. B **97**, 134403 (2018).
[41] F. N. Rybakov, A. B. Borisov, S. Blügel, and N. S. Kiselev, New J. Phys. **18**, 045002 (2016).
[42] A. Varanytsia, G. Posnjak, U. Mur, V. Joshi, K. Darrah, I. Musevic, S. Copar, and L.-C. Chien, Sci. Rep. **7**, 16149 (2017).
[43] A. B. Butenko, A. A. Leonov, U. K. Rößler, and A. N. Bogdanov, Phys. Rev. B **82**, 052403 (2010).
[44] M. N. Wilson, A. B. Butenko, A. N. Bogdanov, and T. L. Monchesky, Phys. Rev. B **89**, 094411 (2014).
[45] J. Rowland, S. Banerjee, and M. Randeria, Phys. Rev. B **93**, 020404 (2016).
[46] U. R. Rößler, A. N. Bogdanov, and C. Pfleiderer, Nature (London) **442**, 797 (2006).
[47] P. Oswald and P. Pieranski, *Nematic and Cholesteric Liquid Crystals: Concepts and Physical Properties Illustrated by Experiments* (CRC Press, Boca Raton, FL, 2005).
[48] M. Kleman and O. D. Lavrentovich, *Soft Matter Physics: An Introduction* (Springer-Verlag, New York, 2003).
[49] A. Hubert and R. Schäfer, *Magnetic Domains* (Springer, Berlin, 1998).
[50] P. J. Ackerman, Z. Qi, and I. I. Smalyukh, Phys. Rev. E **86**, 021703 (2012).
[51] H. R. O. Sohn, P. J. Ackerman, T. J. Boyle, G. H. Sheetah, B. Fornberg, and I. I. Smalyukh, Phys. Rev. E **97**, 052701 (2018).
[52] A. O. Leonov, I. E. Dragunov, U. K. Rößler, and A. N. Bogdanov, Phys. Rev. E **90**, 042502 (2014).
[53] X.-X. Zhang, A. S. Mishchenko, G. De Filippis, and N. Nagaosa, Phys. Rev. B **94**, 174428 (2016); X.-X. Zhang and N. Nagaosa, New J. Phys. **19**, 043012 (2017).
[54] P. G. de Gennes, in *Fluctuations, Instabilities, and Phase Transitions*, edited by T. Riste, NATO Advanced Studies Institute, Ser. B: Physics (Plenum, New York, 1975), Vol. 2, pp. 1–18.